Plasmonics (2013) 8:1221–1226
DOI 10.1007/s11468-013-9535-9

# Optical Magnetic Resonances in Subwavelength Ag–$MgF_2$–Ag Grating Structures

**Eunice Sok Ping Leong · Yan Jun Liu · Chan Choy Chum · Jing Hua Teng**

Received: 23 January 2013 / Accepted: 25 February 2013 / Published online: 8 March 2013


**Abstract** Optical magnetic responses were demonstrated in subwavelength Ag–$MgF_2$–Ag grating structures for transverse magnetic-polarized light. The subwavelength Ag–$MgF_2$–Ag grating structures were fabricated using e-beam lithography followed by a lift-off process. By fixing the Ag–$MgF_2$–Ag strip dimension, the effect of the stripe width on the magnetic resonances was compared for two different grating pitches. With further reduced grating pitch, we pushed the optical magnetic resonances to near UV (deep blue). Numerical simulations confirmed our experimental observations and were in good agreement with the experimental results.

**Keywords** Optical magnetic response · Subwavelength grating · Metamaterials · Permeability

## Introduction

In most natural materials, the magnetic response (susceptibility) is very small in comparison to the electric susceptibility in optical range. The emerging metamaterials fundamentally change the light–matter interactions with both magnetic and electric components of light playing important roles. Comparatively, it is much more challenging to achieve negative permeability $\mu$ than negative permittivity $\varepsilon$ due to the metallic dielectric function and surface plasmon resonances inherent in most of the metamaterials structures. A well-known structure possessing negative $\mu$ is the split ring resonator (SRR) [1]. The SRR consists of one or more metallic loops with small gaps created to simulate the response of an inductive–capacitive (*LC*) resonator circuit when excited with a magnetic field perpendicular to the surface of the ring. Unfortunately, SRRs alone have not been able to achieve resonance frequencies beyond the near infrared [2]. In order to generate the magnetic resonance in the visible range, other structures, such as coupled nanorods [3] or nanostrips [4–6], have been proposed and experimentally tested [7–10].

For the magnetic metamaterials at visible wavelengths, the selection of materials is quite limited. Shalaev et al. exploited Ag–$Al_2O_3$–Ag coupled nanostrips and demonstrated the optical magnetic resonances near 500 nm [8]. Aluminum is generally considered as the best optical materials for UV range since it has low absorption down to 200 nm due to its free electron-like character and high bulk plasmon frequency [11]. Thus far, magnetic metamaterials in the blue range have been demonstrated using Al–$Al_2O_3$–Al nanostructures [12]. However, fabrication of such structures is still very challenging and limited. More importantly, to achieve magnetic resonances in the UV or near UV range, the optical loss of dielectric materials will be a major concern. In this sense, $MgF_2$ stands out due to its excellent transparency (>90 % in transmittance) across the whole UV–Vis–IR range. In addition, $MgF_2$ has good interface adhesion with Ag film [13].

In this paper, we report subwavelength Ag–$MgF_2$–Ag grating structures fabricated using e-beam lithography and lift-off process. Magnetic resonance at deep blue (440 nm) was experimentally demonstrated and verified by numerical simulation for a grating pitch of 190 nm and strip width of 55 nm. The effect of the grating parameters on the magnetic

E. S. P. Leong (✉) · Y. J. Liu · C. C. Chum · J. H. Teng (✉)
Institute of Materials Research and Engineering, Agency for Science, Technology and Research (A*STAR), 3 Research Link, Singapore 117602, Singapore
e-mail: leonge@imre.a-star.edu.sg
e-mail: jh-teng@imre.a-star.edu.sg

resonance of the Ag–MgF2–Ag grating structure is also discussed.

## Experiments and Simulations

### Sample Fabrication

Figure 1 shows the process flow (five steps in brief) of the sample fabrication. A 15×15×0.4 mm quartz substrate with refractive index of 1.46 was cleaned with acetone and isopropyl alcohol (IPA) in an ultrasonic bath. A 10 nm thick indium tin oxide (ITO) layer was first sputtered onto the quartz surface using UBM sputtering system (Nanofilm). The purpose of the ITO layer is to provide a conductive surface on the quartz substrate for e-beam writing. To fabricate the grating structure via e-beam lithography technique, a positive resist, PMMA 950 k with refractive index ~1.49, was spin-coated on the ITO/quartz to form a resist layer with the thickness of 250 nm (step 1). Prebaking was carried out at 170 °C for 15 min. E-beam lithography was carried out with ELIONIX ELS-7000 (step 2). The current and voltage used were 20 pA and 100 kV, respectively. The fabricated patterns consisted of gratings with stripes width of 50−100 nm and pitches of 200−400 nm. Each pattern area was 150×150 μm$^2$. Pattern development was done in MIBK/IPA (1:3) for 70 s (step 3). A short descum was carried out to remove any residual resist on the substrate using RIE Etcher (Plasmalab 80plus, Oxford) at 60 mTorr chamber pressure, 60 W electric power, 60 sccm oxygen flow rate for 5 s. The Ag–$MgF_2$–Ag films were deposited by thermal evaporator (Edwards Auto306). It is known that Ag film deposited on quartz substrates by thermal and e-beam evaporation tends to have a rough surface, and a seed layer can improve the surface roughness greatly. Figure 2 shows the typical surface morphologies of Ag films in our control experiments. From Fig. 2, we can see that compared to the Ag film directly evaporated on the quartz substrate (Fig. 2a), the Ge seed layer improves the surface roughness ($\delta$) of the Ag film (Fig. 2b). Furthermore, it can further reduce the grain size and improve the surface roughness (Fig. 2c) with the liquid nitrogen ($LN_2$) cooled substrate holder. Therefore, to achieve a smoother surface, Ge (2 nm)–Ag (45 nm)–$MgF_2$ (40 nm)–Ag (45 nm) films were thermally evaporated in sequence using a $LN_2$ cooled substrate holder (step 4). The deposition rate for each layer was controlled to 8± 2 nm/min. Finally, Ge–Ag–$MgF_2$–Ag subwavelength grating structures were obtained by a lift-off process (step 5).

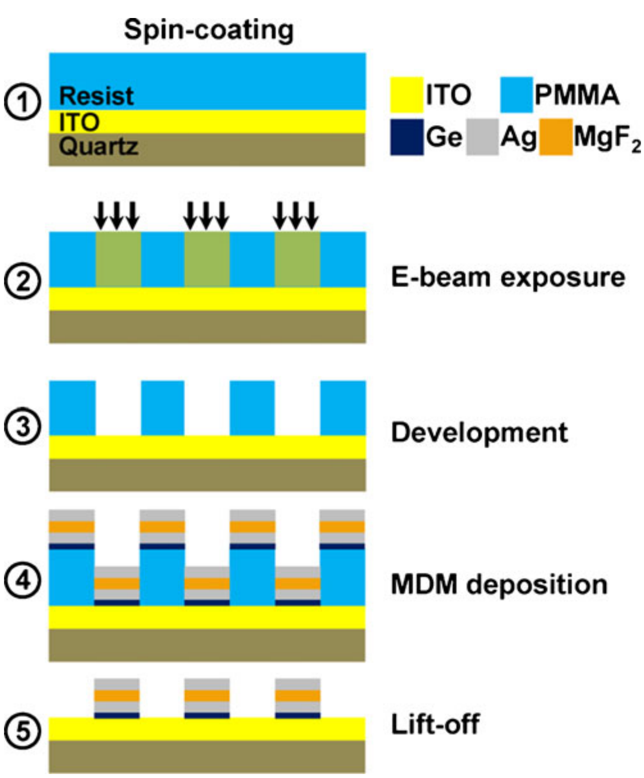


**Fig. 1** (Color online) Schematic of the fabrication process using E-beam lithography. MDM is referring to the metal-dielectric-metal film of Ag–$MgF_2$–Ag

### Spectra Measurement

Optical reflectance and transmission spectra were measured with a polarized probe light beam at normal incidence using a UV–Vis–NIR microspectrophotometer (CRAIC QDI 2010™). The probe light beam was focused to have a detecting area of 7.1×7.1 μm$^2$ using a 36× objective lens combined with a variable aperture.

### Simulations

Numerical simulations of the 1D metal-dielectric-metal (MDM) grating were carried out using finite-difference time domain (FDTD, Lumerical) method. In our previous reports, we found that the surface morphology of Ag film strongly affected the effective permittivity and optical properties in Ag–$MgF_2$–Ag thin film systems [14, 15]. In order to obtain the effective permittivity, we first get the Ag permittivity using the Drude-Lorentz model as reported in [16, 17],

$$\varepsilon_{Ag}(\omega) = \varepsilon_1 - \frac{\omega_p^2}{\omega^2 + i\gamma_p\omega} + \sum_{m=1}^{5} \frac{f_m\omega_m^2}{\omega_m^2 - \omega^2 - i\gamma_m\omega}, \qquad (1)$$

where, $\varepsilon_1$ describes the contribution of electrons from *d*-band to the conduction band [18–20] and varies in our samples; $\gamma_p$ is the damping rate, which is affected by the scattering of electrons due to defects and grain boundaries [16, 17, 21] and it is linearly proportional to $1/r$, where $r$ is the radius of the particle. It is also noted that Ag oxidization plays an important role in affecting the effective refractive

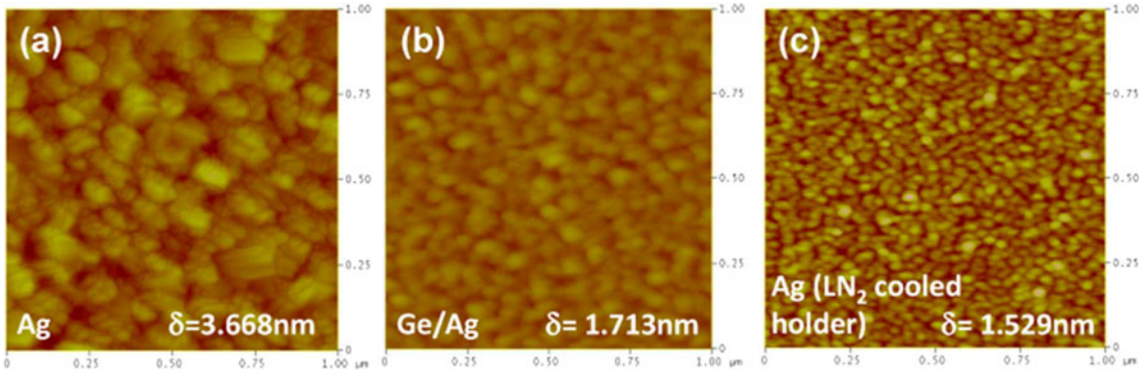


**Fig. 2** (Color online) Surface morphologies for typical $1 \times 1\ \mu m^2$ regions of Ag films evaporated on the quartz substrate directly (**a**), with a Ge seed layer (**b**), and with a Ge seed layer on a $LN_2$ cooled substrate

index of Ag films. Therefore, the effective permittivity, $\varepsilon(\omega)$, of Ag is then obtained from the Maxwell–Garnett equation [17, 22, 23],

$$\frac{\varepsilon(\omega) - \varepsilon_{Ag_2O}(\omega)}{\varepsilon(\omega) + 2\varepsilon_{Ag_2O}(\omega)} = f\,\frac{\varepsilon_{Ag}(\omega) - \varepsilon_{Ag_2O}(\omega)}{\varepsilon_{Ag}(\omega) + 2\varepsilon_{Ag_2O}(\omega)} \tag{2}$$

The refractive index of $MgF_2$ follows a Lorentz–Lorentz formula as listed in [24]. In our simulation, the fitting parameters we used are $f$=55 % in Eq. (2), $\varepsilon_{1,\mathrm{bottom}}$=5.5, $\gamma_{\mathrm{p,bottom}}$=0.25 eV and $\varepsilon_{1,\mathrm{top}}$=3, $\gamma_{\mathrm{p,top}}$=0.55 eV in Eq. (1), where the subscript bottom refers to the bottom Ag layer in contact with the substrate and top refers to the top Ag layer in contact with air. The measured and simulated transmission and reflection spectra of the Ag–$MgF_2$–Ag films are shown in Fig. 3. A close match is observed between the experimental and simulation results. The effective refractive index for the top and bottom Ag layer is then used in the FDTD simulation of the MDM grating structure. A unit cell of the structure was used in the simulation with periodic boundary condition in the $x$-direction and PML boundary condition in the $y$-direction. A plane wave source with either transverse electric (TE) and transverse magnetic (TM) polarization was excited from the bottom of the quartz substrate. The displacement fields were calculated using the displacement field analysis group function in the Lumerical software and plotted with Matlab. For the magnetic permeability retrieval, we performed two calculations for different source direction to get $s$-parameter including $s_{11}$, $s_{12}$, $s_{21}$, and $s_{22}$. Then, following the equations (Eqs. 29–35) in [25], we obtained the effective magnetic permeability for our 1D MDM gratings. It is noted that only the first order grating was used in the calculation of the effective material properties.

## Results and Discussion

To ease the fabrication and validate our numerical analysis, we first fabricated two batches of samples with the pitches of 280 and 380 nm, as shown in Fig. 4a and b. In these two samples, we fixed the width of the MDM stripes at ~108 nm and changed the width of trench from 172 to 272 nm. We measured the transmission and reflection spectra of these two samples for both TE and TM modes, as shown in Fig. 4c and d. As expected, for TE mode, there is neither surface plasmon resonance effect nor magnetic resonance since there is no component of the magnetic field perpendicular to the face of our MDM structure. Therefore, the TE spectra display a nonresonant wavelength dependence over a broad wavelength range, which is very similar to that of a flat silver film. When we excite the sample with light that contains the magnetic field polarized along the $y$-direction, i.e., TM mode, strong resonances from both transmission

**Fig. 3** (Color online) Experimental (**a**) and simulated (**b**) transmission and reflection of the MDM thin film system

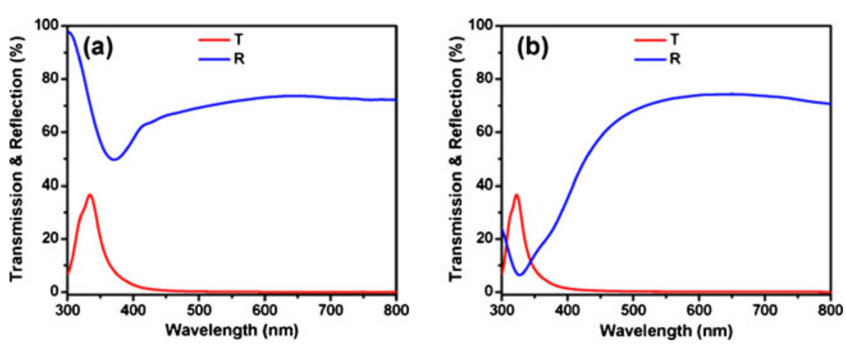

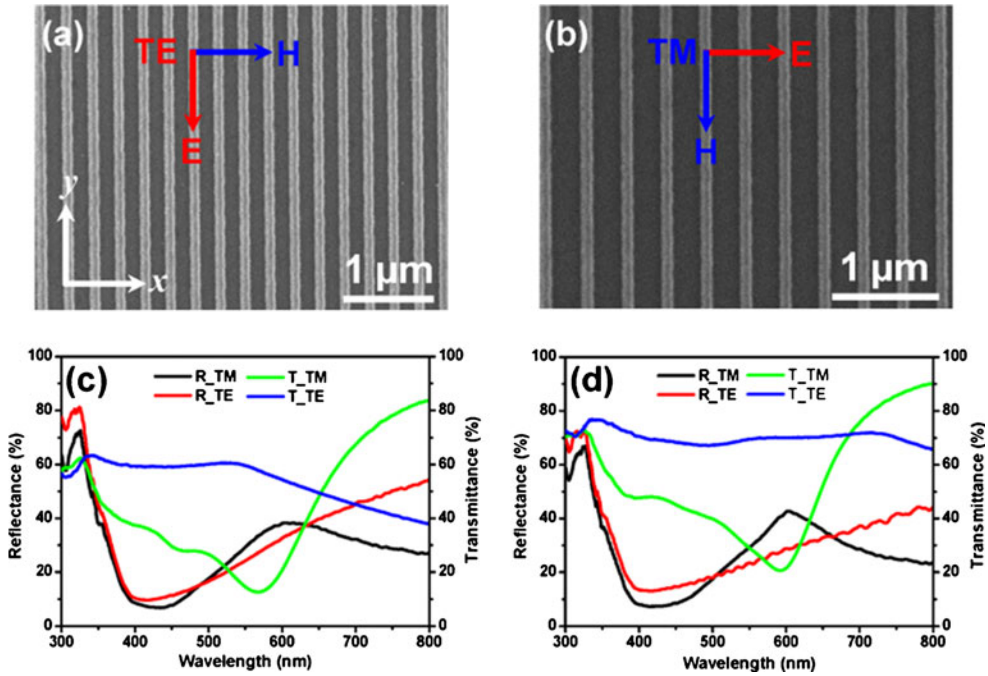


**Fig. 4** (Color online) SEM images of two samples with the pitches of **a** 280 and **b** 380 nm. **c** and **d** are corresponding transmission and reflection spectra measured for both TM- and TE-polarized probe light

and reflection spectra are observed in Fig. 4c and d, which could be attributed to either an electric or magnetic resonance or both.

A further close look at the spectra in Fig. 4c and d for TM polarization reveals important features at two distinct characteristic wavelengths, i.e., two dips, which are attributed to the magnetic resonance and the electric resonance, respectively [8]. To further confirm the nature of the response, we took the structure in Fig. 4a as a representative coupled nanostrip sample and ran FDTD simulations to see the field distribution inside the MDM structures. Figure 5a shows the simulated transmission spectra for TM-polarized light, which roughly match the experimental results in terms of dip and peak positions. The difference between simulated

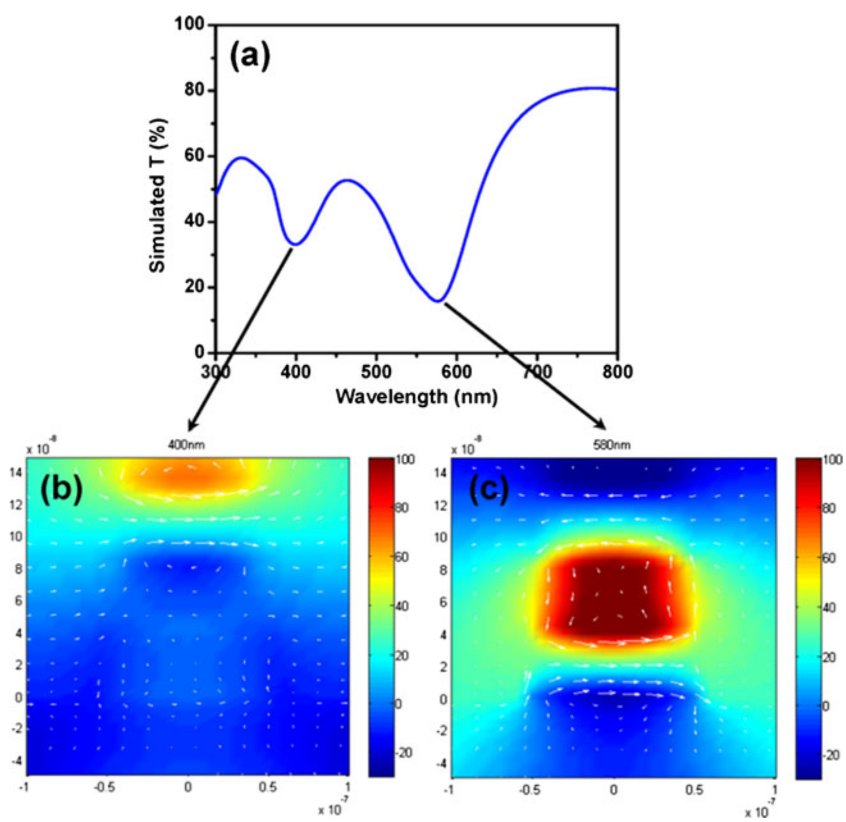


**Fig. 5** (Color online) Simulated transmission spectra of the sample with the pitch of 380 nm for TM-polarized light (**a**), and the field distribution at the two resonant wavelengths of 400 nm (**b**) and 580 nm (**c**)

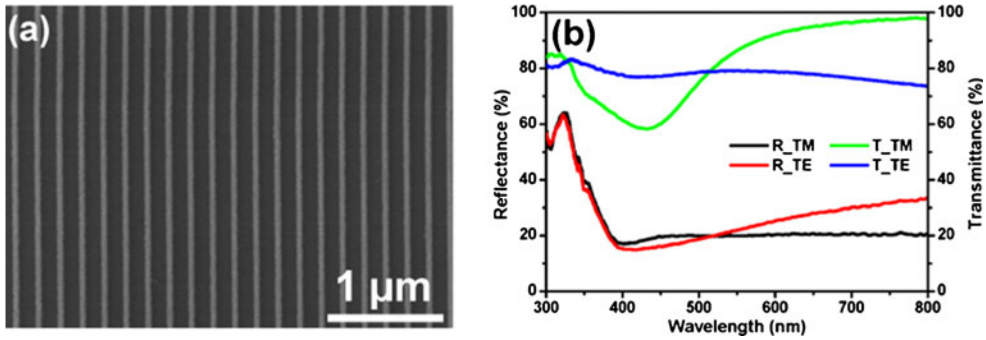


**Fig. 6** (Color online) SEM image (**a**) and corresponding transmission and reflection spectra (**b**) for the MDM structure with the pitch of 190 nm and the ridge width of 55 nm

(Fig. 5a) and experimental (Fig. 4c) results could be attributed to surface roughness and perfectness of the grating. Furthermore, Fig. 5b and c illustrates the field distribution at the two resonance wavelengths of 400 and 580 nm (two dips). The arrows represent the electric displacement whereas the color map represents the magnetic field. At the wavelength of 580 nm, we note that the electric displacement forms a loop resulting in an artificial magnetic moment. We also note a strong magnetic field inside the loop. Therefore, the response at 580 nm is attributed to the magnetic response of the structure. While at the wavelength of 400 nm, the electric displacement is predominantly aligned along one direction with a small circulating component. The magnetic field is also lower when compared to the magnetic resonance. Therefore, the response at 400 nm is attributed to the electric response of the structure.

Optical magnetic resonance is our particular interest in such MDM structures. We therefore retrieved the effective permeability $\mu$ of each sample around the magnetic resonance wavelength $\lambda_m$ using numerical simulations [25]. The values of permeability $\mu$ are 0.4 and 0.5 for the samples with the pitches of 280 and 380 nm, respectively. Both values are less than unity, as opposed to conventional optical materials. Further numerical simulation reveals that for a fixed strip width, the permeability value increases with the increase of the trench width.

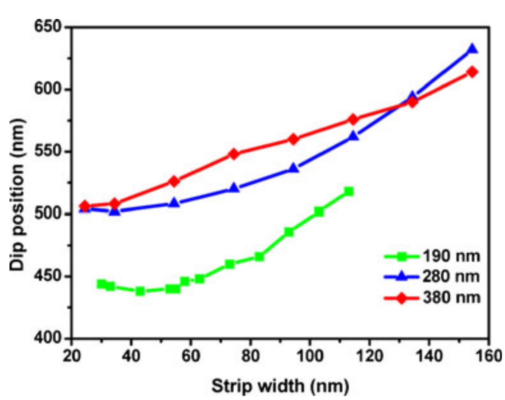


**Fig. 7** (Color online) Effect of the MDM ridge width on the magnetic resonance wavelength for three different pitches

Shalaev et al. have achieved magnetic resonances covering the majority of the visible spectrum (491−754 nm). However, it is still challenging to achieve near UV band based on Ag–$Al_2O_3$–Ag since $Al_2O_3$ has a non-negligible optical loss below 500 nm (transmittance, <80 %). To demonstrate the magnetic resonance at wavelength shorter than 491 nm, the grating dimension has to be further reduced. Given our fabrication ability and the ease of lift-off process, we fabricated the Ag–$MgF_2$–Ag structure with the pitch of 190 nm and the ridge width of 55 nm. Figure 6a and b show the SEM and corresponding transmission and reflection spectra. As shown in Fig. 6b, a magnetic response at 440 nm is successfully achieved, which is also confirmed through our FDTD simulation. At this magnetic resonance wavelength, the retrieved permeability is 0.85.

Based on the validated simulation parameters, we further investigated the effect of stripe width on the magnetic resonance. Figure 7 plots the dependence of the magnetic resonance wavelength on the MDM stripe width for three different pitches. From Fig. 7, for a larger pitch, the magnetic resonance wavelength is almost linearly correlated with the stripe width. However, for a smaller pitch, the MDM structures exhibit saturation due to size scaling, indicating that there exists an optimum value. From the simulation, with the pitch of 190 nm and the ridge width of 43 nm, optical magnetic resonance at 438 nm could be achieved. From the above discussion, the size scaling induced saturation point limits us to further push the optical magnetic resonances to deep UV band for Ag-based MDM grating structure. One has to choose other materials (e.g., aluminum) to achieve optical magnetic resonances in UV or deep UV band.

## Conclusion

In summary, we have demonstrated optical magnetic responses in subwavelength Ag–$MgF_2$–Ag grating structures for TM-polarized light. The resonant properties were studied both experimentally and numerically. By fixing the Ag–$MgF_2$–Ag strip dimension, the effect of the stripe width on the magnetic resonances was compared for two different grating pitches. Due to the excellent transparency of $MgF_2$, we can push the optical magnetic resonances to 440 nm by shrinking the grating pitch. Numerical investigation showed that there exists a saturation point due to size scaling when we push the magnetic resonance to the near UV band. Our results showed that the coupled Ag–$MgF_2$–Ag nanostrip structure is particularly useful for producing controllable optical magnetism in the UV or near UV band.

**Acknowledgments** This work was financially supported by Agency for Science, Technology and Research (A*STAR), under grant no. 0921540099 and 0921540098. ESP Leong would like to thank Dr Bing Wang for technical discussion and the Lumerical support team for their help.

## References

1. Pendry JB, Holden AJ, Robbins DJ, Stewart WJ (1999) IEEE Trans Microw Theory Tech 47:2075
2. Klein MW, Enkrich C, Wegener M, Soukoulis CM, Linden S (2006) Opt Lett 31:1259
3. Podolskiy VA, Sarychev AK, Shalaev VM (2002) J Nonlinear Opt Phys Mater 11:65
4. Kildishev AV, Cai W, Chettiar UK, Yuan H-K, Sarychev AK, Drachev VP, Shalaev VM (2006) J Opt Soc Am B 23:423
5. Shvets G, Urzhumov YA (2006) J Opt A 8:S122
6. Chettiar UK, Kildishev AV, Klar TA, Shalaev VM (2006) Opt Express 14:7872
7. Yuan H-K, Chettiar UK, Cai W, Kildishev AV, Boltasseva A, Drachev VP, Shalaev VM (2007) Opt Express 15:1078
8. Cai W, Chettiar UK, Yuan H-K, de Silva VC, Kildishev AV, Drachev VP, Shalaev VM (2007) Opt Express 15:3333
9. Xiao S, Chettiar UK, Kildishev AV, Drachev V, Khoo IC, Shalaev VM (2009) Appl Phys Lett 95:0331115
10. Kaplan AF, Chen Y-H, Kang M-G, Guo LJ, Xu T, Luo X (2009) J Vac Sci Technol B 27:3175
11. Palik ED, Ghosh G (1998) Handbook of optical constants of solids. Elsevier, New York
12. Jeyaram Y, Jha SK, Agio M, Loffler JF, Ekinci Y (2010) Opt Lett 35:1656
13. Xu X, Tang Z, Shao J, Fan Z (2005) Appl Surf Sci 245:11
14. Leong ESP, Liu YJ, Wang B, Teng JH (2011) ACS Appl Mater Interfaces 3:1148
15. Leong ESP, Liu YJ, Chum CC, Wang B, Teng JH (2012) Appl Phys A 107:127
16. Drachev VP, Chettiar UK, Kildishev AV, Yuan HK, Cai WS, Shalaev VM (2008) Opt Express 16:1186
17. Chen WQ, Thoreson MD, Ishii S, Kildishev AV, Shalaev VM (2010) Opt Express 18:5124
18. Wang ZG, Cai X, Chen QL, Li LH (2006) Vacuum 80:438
19. Pinchuk A, Kreibig U, Hilger A (2004) Surf Sci 557:269
20. He Y, Zeng T (2010) J Phys Chem C 114:18023
21. Hovel H, Fritz S, Hilger A, Kreibig U, Vollmer M (1993) Phys Rev B 48:18178
22. Zhang JZ, Noguez C (2008) Plasmonics 3:127
23. Dalacu D, Martinu L (2001) J Opt Soc Am B 18:85
24. https://www.cvimellesgriot.net/Products/Documents/Technical-Guide/Optical-Coatings.pdf.
25. Smith DR, Vier DC, Koschny T, Soukoulis CM (2005) Phys Rev E 71:036617